Available online at www.sciencedirect.com
ScienceDirect
Journal of Sound and Vibration 322 (2009) 393–400
JOURNAL OF SOUND AND VIBRATION
www.elsevier.com/locate/jsvi

The number of limit cycle bifurcation diagrams for the generalized mixed Rayleigh–Liénard oscillator

Q. Ding[a,*], A.Y.T. Leung[b]

[a]Department of Mechanics, Tianjin University, 300072, PR China
[b]Department of Building and Construction, City University of Hong Kong, China

Received 11 March 2008; received in revised form 2 November 2008; accepted 9 November 2008
Handling Editor: J. Lam
Available online 23 December 2008

Abstract

This paper investigates the generalized mixed Rayleigh–Liénard oscillator with highly nonlinear terms. Not restrict to the number of limit cycles, this analysis considers mainly the number of limit cycle bifurcation diagrams of the system. First, the singularity theory approach is applied to the first-order averaged approximation of the system with lower-order nonlinear terms to reveal all possible bifurcation diagrams. By summarizing the generating rule and structural distinction of different bifurcation diagrams, a numerical procedure is then developed. Calculation suggests that the number of bifurcation diagrams increase very fast as the order of nonlinear terms. Lastly, numerical simulations are adopted to approve the analytical results.

1. Introduction

The periodic solutions of autonomous nonlinear dynamical systems are defined as limit cycles, which are also described as the self-excited oscillations to distinguish them from oscillations induced by a time-dependent forcing function. The limit cycles have been observed in a wide variety of biological, chemical, electrical and mechanical systems. Most of the early history in the theory of limit cycles was stimulated by practical problems displaying periodic behavior. Rayleigh [1] discussed the differential equation related to the oscillation of a violin string. Following the invention of the triode vacuum tube, which was able to produce stable self-excited oscillations with constant amplitude, the well-known differential equation which describes this phenomenon was obtained by van der Pol [2]. Then, Liénard [3] generalized the van der Pol system as the most famous class of differential equations. The Liénard equation, which is often taken as the typical example of nonlinear self-excited vibration problem, can be used to model resistor–inductor–capacitor circuits with nonlinear circuit elements. It can also be used to model certain mechanical systems which contain the nonlinear damping coefficients and the restoring force or stiffness.

*Corresponding author. Tel.: +8622 27401099.
E-mail addresses: qding@tju.edu.cn (Q. Ding), bcaleung@cityu.edu.hk (A.Y.T. Leung).

0022-460X/$ - see front matter © 2008 Elsevier Ltd. All rights reserved.
doi:10.1016/j.jsv.2008.11.014

Limit cycles usually arise at a Hopf bifurcation in nonlinear systems with varying parameters. In mechanical systems, the varying parameter is frequently a damping coefficient. Regular or normal limit cycles are distinguished from large-amplitude limit cycles. Stable normal limit cycles are created at a supercritical Hopf bifurcation with the limit cycle amplitude building up gradually from nought as the parameter is varied from the Hopf bifurcation point. So they are also called small-amplitude limit cycles. In contrast, stable large-amplitude limit cycles are either created at a subcritical Hopf bifurcation with finite amplitude or show a sudden increase (jump) in amplitude after originating as a normal limit cycle at a Hopf bifurcation point.

The nonlinear dynamical systems can either be strongly or weakly nonlinear. Generally, the damping terms are considered to be weakly nonlinear. So the restoring or stiffness terms determine whether the nonlinearity of a system is strong or weak. For the weakly nonlinear oscillators, the weakly nonlinear terms are multiplied by a small positive parameter ε as an indication. Letting $\varepsilon = 0$ results the generating equations, and their solutions are generating solutions. For strongly nonlinear oscillators, there are more than one generating solutions or equilibriums. The limit cycles can exist both inside and outside the potential wells.

As a particular case of the second part of Hibert's sixteenth problem [4], lots of papers discussed the possible number of limit cycle of Liénard or generalized mixed Rayleigh–Liénard oscillator recently using the Jacobian elliptic functions. Chen et al. [5,6] presented two elliptic function methods, the elliptic perturbation method and the elliptic Linstedt–Poincare method, to calculate the higher-order approximations, which converge to the exact equation of each limit cycle, for the equations with strong nonlinear stiffness. Garcia-Margallo and Bejarano [7] applied the Jacobian elliptic functions with the generalized harmonic balance method for the generalized mixed Rayleigh–Liénard differential equations with positive linear and nonlinear stiffnesses. They showed that when the damping coefficient is of degree 4, there is either zero, one or two limit cycles around the origin. They [8] also showed that the system with two potential wells can have six limit cycles. Zhang and Yu [9] used the Melnikov and Petrov methods to study the limit cycles associated with a generalized codimension-3 Liénard oscillator. Local and global bifurcations for the surge oscillations in axial flow compressors and wing rock oscillations in aircraft flight dynamics were discussed by Lynch and Christopher [10]. They developed an algebraic method for determining the Liapunov quantities, to compute the maximum number of small-amplitude limit cycles that can bifurcate within a small neighborhood of the system origin. Both the small-amplitude and large-amplitude limit cycle bifurcations were discussed with considering the damping coefficient is of degree 14. Application of secondary bifurcations to large amplitude limit cycles in axial flow compressors and wing rock oscillations in aircraft flight dynamics were also analyzed by Ananthkrishnan et al. [11].

It is well known that as the bifurcation parameter is increased and then decreased, a hysteresis loop is formed on branches of the smallest and the largest stable limit cycles through a series of saddle-node bifurcations (jumps). More or less central stable limit cycles are not involved in the loop. Due to different bifurcation diagrams results not only different hysteresis loops but also different number of limit cycles that can be encountered during normal operation, the number of limit cycle bifurcation diagrams is worth to be investigated. To the authors' knowledge, this problem has seldom been dealt with for the systems with highly nonlinear terms.

Singularity theory developed in 1960s enables us to deal with various local static bifurcation problems [12,13]. The theory comprises three parts, recognition, unfolding and classification by codimension. Applying the singularity theory approach to bifurcation equations, the qualitative types of solution sets (i.e., bifurcation diagrams) can be obtained. As a result, both the number of possible limit cycles and the number of possible limit cycle bifurcation diagrams can be determined.

This paper investigates the generalized mixed Rayleigh–Liénard oscillator using the averaging method and the singularity theory. Because the singularity theory approach can be only applied to the system with lower-order nonlinear terms, the structural distinctions of different bifurcation diagrams are summarized and a numerical procedure is then developed to calculate the number of limit cycle bifurcation diagrams of the system with highly nonlinear terms. Numerical simulation is also adopted to approve the results.

2. Averaging procedure

Consider the generalized mixed Rayleigh–Liénard oscillator as

$$\ddot{x} + \varepsilon f(x, \dot{x}, \mu)\dot{x} + g(x, \mu) = 0 \tag{1}$$

where ε is a small, positive parameter, and μ is a set of k-parameters which characterize the dynamical system. The weakly nonlinear terms, f and g, are generally even and odd degree polynomials, respectively,

$$g(x,\mu)=x+\varepsilon a x^3,\quad f(x,\dot{x},\mu)=\lambda+\left(\sum_{i=1}^{n} b_{2i}x^{2i}+c\dot{x}^2\right) \tag{2}$$

where a, c and b_{2i} are constants, and λ is taken as the bifurcation parameter in bifurcation analysis. Generally the damping coefficient is of degree 4, i.e., $n=2$. But in determining the number of limit cycles, the possibilities when $n=7$ was studied as an example in Ref. [10].

To obtain the bifurcation equation, we apply the averaging procedure to Eq. (1). Rearrange (1), in consideration of Eq. (2), in the following form [14]

$$\ddot{x}+x=\varepsilon\left[-ax^3+\left(\lambda+\sum_{i=1}^{n} b_{2i}x^{2i}+c\dot{x}^2\right)\dot{x}\right] \tag{3}$$

Transforming the dependent variable from x to A and θ where

$$x=A\cos\psi,\quad \dot{x}=-A\sin\psi,\quad \psi=t+\theta$$

the standard form of the equation governing A and θ is deduced as

$$\begin{aligned}\frac{\mathrm{d}A}{\mathrm{d}t}&=\varepsilon\frac{A}{2}\left[\lambda+\sum_{i=1}^{n} b_{2i}A^{2i}(1-\cos 4\psi)\cdot(1+\cos 2\psi)^{i-1}/2^{1+i}+cA^2\sin^4\psi\right]\\ \frac{\mathrm{d}\theta}{\mathrm{d}t}&=\varepsilon\frac{3a}{8}A^3+\varepsilon A\left[\sum_{i=1}^{n} b_{2i}A^{2i}(1+\cos 2\psi)^{i}\cdot\sin 2\psi/2^{1+i}\right]\end{aligned} \tag{4}$$

One finds that the cubic stiffness term, ax^3, influences only the variation of the phase but not the amplitude of response of the autonomous system (3). Using the *Krylov–Bogoliubov* first-order approximation:

$$\begin{aligned}A&=y+\varepsilon U(t,y,\gamma)+O(\varepsilon^2)\\ \theta&=\gamma+\varepsilon V(t,y,\gamma)+O(\varepsilon^2)\end{aligned} \tag{5}$$

where y and γ represent the first-order approximate solution of A and θ in steady-state, respectively. The second equation of (4) can be ignored for it does not influence the possible limit cycles. The right-hand sides of the first equation of (4) is averaged over ψ from 0 to 2π (assuming y and γ are constants), which results

$$\frac{\mathrm{d}y}{\mathrm{d}t}=\frac{y}{2}\left(\lambda+\sum_{i=1}^{n} d_{2i}y^{2i}\right) \tag{6}$$

where $d_2=(b_2+3c)/4$, $d_4=b_4/8$, $d_6=5b_6/64$, $d_8=7b_8/128$, $d_{10}=21b_{10}/512$, $d_{12}=33b_{10}/1024$ and $d_{14}=429b_{14}/16384$. The steady-state response of the averaged system (6) can be obtained by setting $\mathrm{d}y/\mathrm{d}t=0$, which yields the following bifurcation equation

$$G_n(y,\lambda,\Gamma)=y^{2n+1}-\lambda y+\left(\sum_{i=1}^{n-1}\alpha_i y^{2i}\right)y=0 \tag{7}$$

where $\Gamma=\{\alpha_i\}$: $\alpha_i=d_{2i}/d_{2n}$, $i=1,2,\ldots,n-1$ (without loss of generality, suppose $d_{2n}\neq 0$).

3. Singularity theory approach

For cases $n\leqslant 4$, the bifurcation of Eq. (7) can be investigated by the singularity theory. Taking λ as the bifurcation parameter and $\Gamma=\{\alpha_i\}$ the unfolding parameter space, Eq. (7) is proven to be a $(n-1)$-parameter ($n\geqslant 2$), $\mathbf{Z}_2$-symmetric universal unfolding of a family germs $g=y^{2n+1}-\lambda y$, with codimension $n-1$ (the number

of parameters α_i, $i = 1, 2, \ldots, n-1$). By defining $u = y^2$, $G_n = 0$ can be written in the form

$$G_n(y, \lambda, \Gamma) = \left(u^n - \lambda + \sum_{i=1}^{n-1} \alpha_i u^i \right) y = 0 \tag{8}$$

For the case $y \neq 0$, all phenomena occur in pairs—whatever occurs at (y, λ, Γ) is mirrored at $(-y, \lambda, \Gamma)$. Note that y denotes the amplitude of response of the system. So only the case $y > 0$ can be taken as the actual result. There are three sources of non-persistence, i.e., bifurcation, hysteresis, and double limit points, carry over to $y \neq 0$. In Table 1, equations of these three sources are listed as $B_1(\mathbf{Z}_2)$, $H_1(\mathbf{Z}_2)$ and $\mathrm{D}(\mathbf{Z}_2)$, respectively.

For the case $y = 0$, a pitchfork occurs at $\lambda = 0$ from $y = 0$. Analyzing the non-persistent behavior for the pitchfork leads to a bifurcation and a hysteresis sets, $B_0(\mathbf{Z}_2)$ and $H_0(\mathbf{Z}_2)$, respectively, as also listed in Table 1.

It can be proven that the above five sets enumerate all the sources of non-persistence of bifurcations with $\mathbf{Z}_2$-symmetry, and they compose the transition set $\Sigma(\mathbf{Z}_2)$. Analytic expressions are derived using the formulas for various components of $\Sigma(\mathbf{Z}_2)$ for the 1, 2 and 3-parameter, $\mathbf{Z}_2$-symmetric universal unfoldings and are given in Table 2. The transition sets in plane (α_1, α_2) and bifurcation diagrams, that is u changes with bifurcation parameter λ for a set of Γ, are given in Figs. 1 and 2, respectively. For $(n \geqslant 5-1)$-parameter cases, analytic expressions of transition sets are very complex and lengthy (except $H_0(\mathbf{Z}_2)$ which is always equal to $\alpha_1 = 0$) and difficult to deal with on planar space.

Two bifurcation diagrams of $G_2 = 0$, i.e. (1) and (2) in Fig. 2, represent the basic modes of bifurcation (i.e., normal Hopf bifurcations). The mode 1 indicates a super-critical Hopf bifurcation wherein a stable non-trivial solution is created about the unstable equilibrium. The mode 2 indicates a sub-critical Hopf bifurcation wherein an unstable non-trivial solution is created about the stable equilibrium, and a stable non-trivial solution arises through a secondary bifurcation [11]. In other words, there is one non-trivial solution for the mode 1 and there are two non-trivial solutions for the mode 2, respectively. For $G_n = 0$ with $n \geqslant 3$, all bifurcation diagrams besides the two basic modes are generated from them through hysteresis (saddle-node) bifurcations. As a hysteresis bifurcation results two solutions, one stable and another unstable, the largest number of non-trivial solutions of $G_n = 0$ can be acquired to be n through solving Eq. (8). For $G_n = 0$ with odd n, bifurcation diagrams are generated from the mode 1 through $(n-1)/2$ times hysteresis bifurcations.

Table 1
Sources of nonpersistence of n-parameter $\mathbf{Z}_2$-symmetric bifurcations.

$B_1(\mathbf{Z}_2) = \{\Gamma \in R^n | \exists (u, \lambda),\ u > 0$ such that $R = R_u = R_\lambda = 0$ at $(u, \lambda, \Gamma)\}$
$B_0(\mathbf{Z}_2) = \{\Gamma \in R^n | \exists \lambda$ such that $R = R_\lambda = 0$ at $(0, \lambda, \Gamma)\}$
$H_1(\mathbf{Z}_2) = \{\Gamma \in R^n | \exists (u, \lambda),\ u > 0$ such that $R = R_u = R_{uu} = 0$ at $(u, \lambda, \Gamma)\}$
$H_0(\mathbf{Z}_2) = \{\Gamma \in R^n | \exists \lambda$ such that $R = R_u = 0$ at $(0, \lambda, \Gamma)\}$
$D(\mathbf{Z}_2) = \{\Gamma \in R^n | \exists u_1, u_2, \lambda\ (u_1 \neq u_1, u_1, u_1 > 0)$, such that $R = uR_u = 0$ at (u_1, λ, Γ) and $(u_2, \lambda, \Gamma)\}$
$\Sigma(\mathbf{Z}_2) = B_1(\mathbf{Z}_2) \cup B_0(\mathbf{Z}_2) \cup H_1(\mathbf{Z}_2) \cup H_0(\mathbf{Z}_2) \cup D(\mathbf{Z}_2)$

Table 2
Transition sets for the 1, 2 and 3-parameter, $\mathbf{Z}_2$-symmetric bifurcations.

Bifurcation equation	$B_0(\mathbf{Z}_2)$	$B_1(\mathbf{Z}_2)$	$H_0(\mathbf{Z}_2)$	$H_1(\mathbf{Z}_2)$	$D_1(\mathbf{Z}_2)$
$G_2 = 0$	$\emptyset$	$\emptyset$	$\alpha_1 = 0$	$\emptyset$	$\emptyset$
$G_3 = 0$	$\emptyset$	$\emptyset$	$\alpha_1 = 0$	$\alpha_1 = \alpha_2^3/3,\ \alpha_2 \leqslant 0$	$\alpha_1 = \alpha_2^3/4,\ \alpha_2 \leqslant 0$
$G_4 = 0$	$\emptyset$	$\emptyset$	$\alpha_1 = 0$	$\alpha_1 = 3\alpha_3 u^2 + 8u^3$, $\alpha_2 = -3\alpha_3 u - 6u^2$, $u > 0$	$\alpha_1 = 3\alpha_3 u_1 u_2 + 4u_1 u_2 (u_1 + u_2)$ $\alpha_2 = -\frac{3}{2}\alpha_3 (u_1 + u_2) - 2(u_1^2 + u_1 u_2 + u_2^2)$ $u_1 \neq u_2,\quad u_1, u_2 > 0$

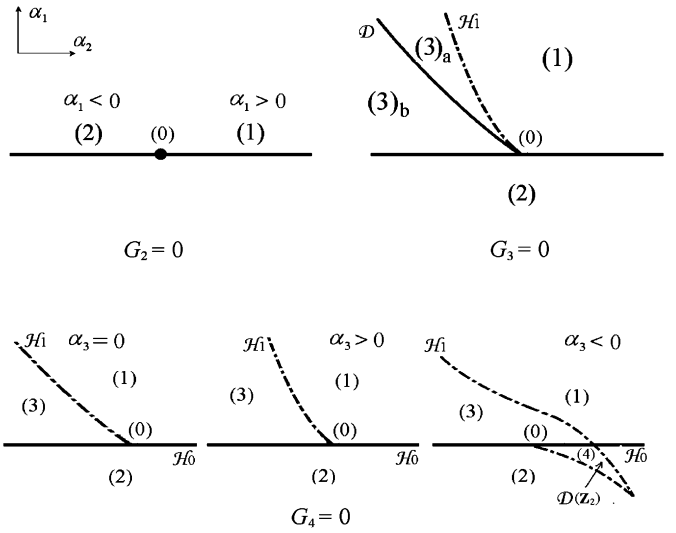

Fig. 1. The transition sets in plane (α_1, α_2) for 1, 2 and 3-parameter, $\mathbf{Z}_2$-symmetric universal unfoldings (G_2, G_3 and G_4).

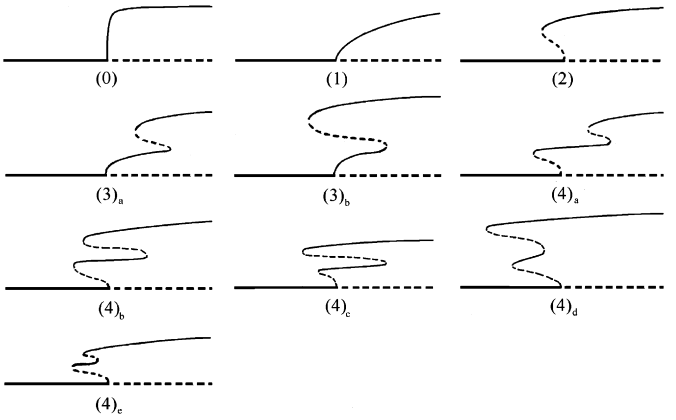

Fig. 2. Bifurcation diagrams corresponding to Fig. 1.

For $G_n = 0$ with even n, bifurcation diagrams are generated from the mode 2 through $(n-2)/2$ times hysteresis bifurcations.

Most relevant articles study only the largest number of limit cycles (non-trivial solutions). In this paper, the number of possible bifurcation diagrams of the generalized mixed Rayleigh–Liénard oscillator with highly nonlinear terms will be discussed based on the singularity analysis for cases $n \leqslant 4$.

4. The number of limit cycle bifurcation diagrams

The bifurcation diagrams $(4)_a$ to $(4)_e$ in Fig. 2 are resulted as the unfolding parameters are differently valued inside the area (4) in Fig 1.Though all of them have one stable trivial solution, two stable non-trivial solutions and two unstable non-trivial solutions, their structures are actually topological different. In the following, we use $N(n)$ to denote the number of bifurcation diagrams of $G_n = 0$. From Fig. 2 one finds that the bifurcation diagrams of $G_n = 0$ include all that of $G_i = 0$, $i = 2, 3, \ldots, n-1$. Denoting the number of new arisen bifurcation diagrams of $G_n = 0$ as $NW(n)$, one has $N(n) = N(n-1) + NW(n)$ or $N(n) = N(2) + \sum_{i=3}^{n} NW(i)$ whereas $N(2) = 2$, which covers the modes 1 and 2 of Fig. 2. For example, one finds that $NW(3) = 2$, which covers the bifurcation diagrams $(3)_a$ and $(3)_b$ of Fig. 2, so $N(3) = N(2) + NW(3) = 4$. Further one finds that $NW(4) = 5$,

which covers the bifurcation diagrams $(4)_a$ through $(4)_e$, so $N(4) = N(3) + NW(4) = 9$. In the following we discuss the calculation of $NW(n)$s for cases $n \geqslant 5$.

For all bifurcation diagrams of Fig. 2, the bifurcation point at the λ axis is denoted as point 1. Ascending along a non-trivial solution curve from the point 1, the hysteresis (or saddle-node) bifurcation points encountered are denoted in sequence as point 2, 3,…, n, respectively. To calculate the number of bifurcation diagrams, two facts are summarized below.

1. For the bifurcations of $G_n = 0$ with even order n, all bifurcation points with odd numbers are left-turn points. A solution branch below the left-turn point is stable and an upper one is unstable. Contrarily for $G_n = 0$ with odd order n, all bifurcation points with odd numbers are right-turn points. A solution branch below the right-turn is unstable and an upper one is stable.
2. Projecting the bifurcation point i on λ axis and denoting it as the projected point λ_i (numerically $\lambda_i = i$), the bifurcation diagrams can be distinguished by the distribution, or sequence, of the projected point λ_i ($i = 1, 2,\ldots, n$). An important fact is that for any right-turn bifurcation point i, its projected point λ_i locates in the left side of, not inevitably next to, the projected points λ_{i-1} and λ_{i+1}. Contrarily for any left-turn bifurcation point i, its projected point λ_i locates in the right side of, not inevitably next to, the projected points λ_{i-1} and λ_{i+1}.

Based on these facts, a numerical procedure is developed to calculate the number of bifurcation diagrams of the generalized mixed Rayleigh–Liénard oscillator (1) with any highly nonlinearity, see the results listed in Table 3 for $n = 4$ to 8. Table 3 indicates that the number of bifurcations increase very fast as the order of nonlinear terms. Some examples are also presented in Table 3 wherein the projected points λ_i's are arranged in a descending order (i.e., from right to left) to compose the representative numbers, RNs. The bifurcation diagrams with RN = 516 324 for $n = 6$ and RN = 2 641 537 for $n = 7$ are sketchily depicted in Fig. 3. The bifurcation with RN = 2 641 537 was also calculated numerically in Ref. [10] as a particular example of limit cycle in highly nonlinear differential equations (the parameters value $a = c = 0$, $b_2 = -90$, $b_4 = 882$,

Table 3
Number of bifurcation diagrams and examples.

Order n	4	5	6	7	8
$NW(n)$	5	16	61	272	1385
RNs	1342	21 435	132 546	2 641 537	15 327 864
	3412	42 513	315 246	4 621 357	37 125 648
			516 342	6 472 135	51 327 648
					78 563 142

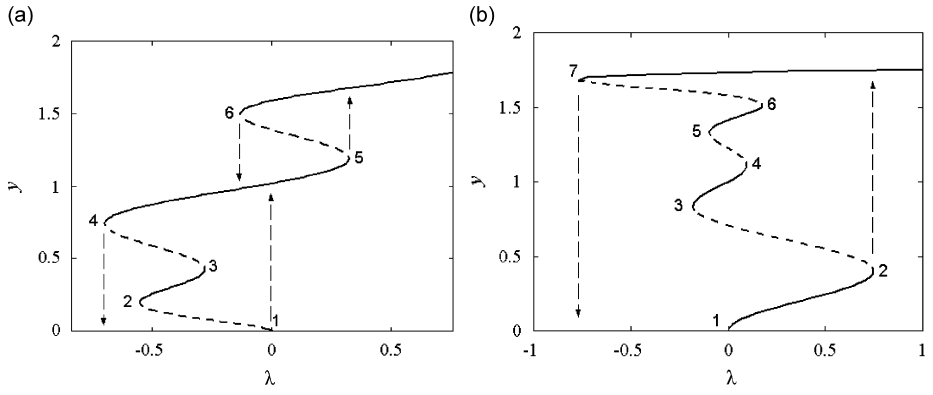

Fig. 3. Bifurcation diagrams of highly nonlinear systems. (a) RN = 516 324 ($n = 6$); (b) RN = 2 641 537 ($n = 7$).

$b_6 = -2598.4$, $b_8 = 3359.997$, $b_{10} = -2133.34$, $b_{12} = 651.638$ and $b_{14} = -76.38$. Note that in Ref. [10] the bifurcation parameter $a_0 = -\lambda$).

Fig. 3(b) shows that in the neighborhood of the normal Hopf bifurcation point $\lambda = 0$, there exist a stable trivial equilibrium (when $\lambda < 0$) and four stable steady-state solutions in different levels (i.e., the limit cycles with small- or large-amplitudes). The values of λ and the initial conditions x_0 and $\dot{x}_0$ determine which solution can be arrived at. To verify the bifurcation analysis, the system (3) was numerically integrated with different values of λ, x_0 and $\dot{x}_0$, see the time histories shown in Fig. 4. The 4th-order Runge–Kutta method was adopted for the integrations. For the system (3), the period length of normal limit cycle is 2π, and the period lengths of limit cycles with large-amplitudes should be longer than 2π. By setting the step-length to be $2\pi/100$ and the maximum error is estimated not larger than 10^{-8}, all solutions were determined exactly.

Referring to Fig. 3, Fig. 4 reflects the following phenomena.

1. As the bifurcation parameter λ is increased and then decreased, a hysteresis loop (outer-loop) is formed on the branches of the smallest and largest stable limit cycles. Fig. 4(a)–(d) and back to 4(a) approve such an outer-loop. From Fig. 4(a) with $\lambda = -0.5$ and $x_0 = 0.5$ (let $\dot{x}_0 = 0.1$ for all cases), one finds that the trivial equilibrium is stable under relative small initial disturbance before the normal Hopf bifurcation is occurred. As λ increases, a normal Hopf bifurcation results the smallest-amplitude limit cycle (i.e., the first level stable

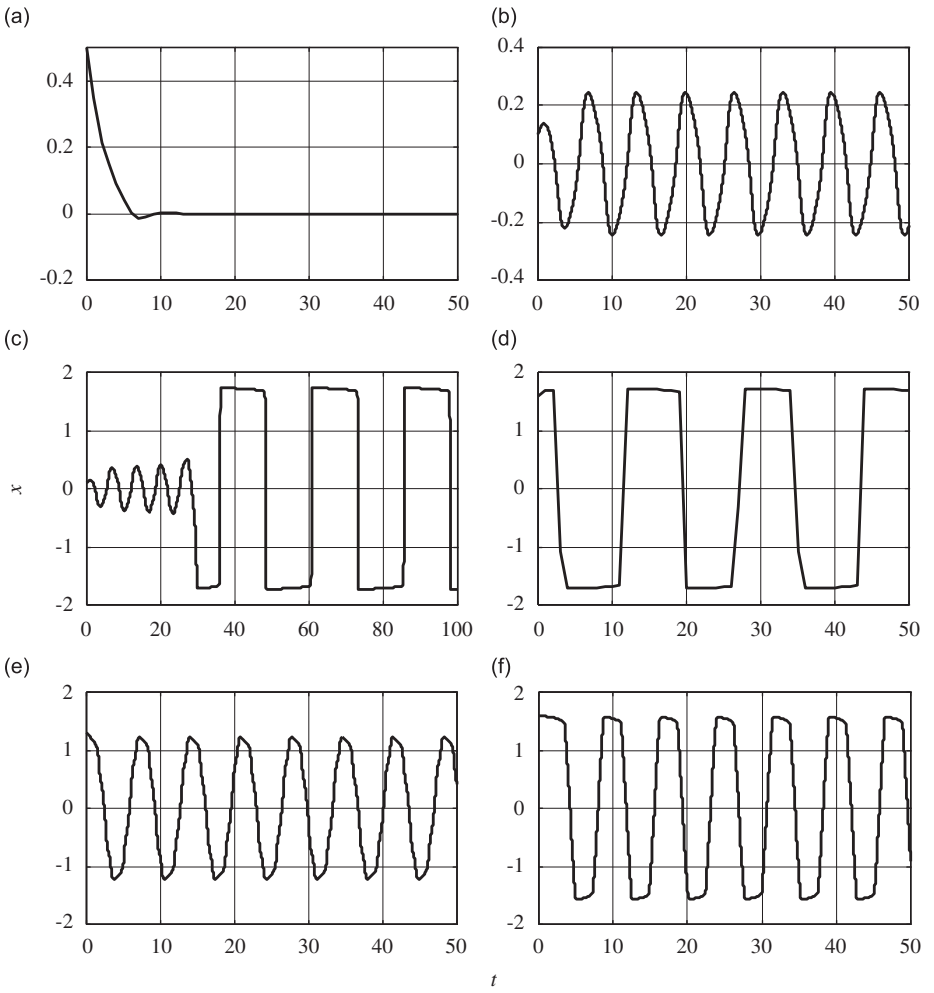

Fig. 4. Time histories of the system (3) with different values of (λ, x_0, $\dot{x}_0$), referring to Fig. 3(b). (a) −0.5, 0.5, 0.1; (b) 0.5, 0.2, 0.1; (c) 1.0, 0.2, 0.1; (d) −0.5, 1.6, 0.1; (e) 0.05, 1.3, 0.1; (f) 0.05, 1.6, 0.1.

non-trivial solution with amplitude being about 0.25), then a hysteresis bifurcation happening at the point 3 results a jump to the largest-amplitude limit cycle (i.e., the fourth level stable non-trivial solution with amplitude being about 1.74), see Fig. 4(b) and (c). Note that in these two cases, the rather small initial conditions means the trivial equilibrium is unstable. As λ is decreased but before the hysteresis bifurcation happens at the point 7, the system stays at the largest stable limit cycle branch all through, see Fig. 4(d) with comparatively larger initial condition ($x_0 = 1.6$). As λ is decreased lower than the point 7, the system will return back to the stable trivial equilibrium.

2. Generally, more or less central stable limit cycles are not involved in the outer-loop. So these limit cycles cannot be encountered during the system's normal operation. Whereas an enough disturbance can lead the system reach to these limit cycle branches. Fig. 4(e) and (f) illustrate the realizations of two middle limit cycles (i.e., the second level and the third level stable non-trivial solutions with amplitude being about 1.23 and 1.58, respectively) under rather large initial conditions at $\lambda = 0.05$.

5. Conclusion

The generalized mixed Rayleigh–Liénard oscillator with highly nonlinear terms has been investigated in this paper. Singularity theory approach is applied to the first-order averaged approximation of the system with lower-order nonlinear terms. Analyzing the limit cycle bifurcation diagrams shows that they are generated from two basic ones, the sub- and super-critical Hopf bifurcations, through hysteresis bifurcations. Different bifurcation diagrams can be structural distinguished from the difference of the projected positions of hysteresis points on the bifurcation parameter axis. Based on this rule, a numerical procedure was developed to calculate the number of bifurcation diagrams of the system with any highly nonlinearity. Calculations suggest that the number of bifurcation diagrams increase very fast as the order of nonlinear terms. Numerical simulations approve the analytical results by presenting both the hysteresis loop between the smallest and largest stable limit cycles as the bifurcation parameter is increased and decreased and realizations of the middle limit cycles under certain initial conditions.

Acknowledgement

This research was supported by the NNSF of PR China under Grant #10672115 and 10632040.

References

[1] J. Rayleigh, *The Theory of Sound*, Dover, New York, 1945.
[2] B. van der Pol, On relaxation-oscillations, *Philosophical Magazine* 7 (901–912) (1926) 946–954.
[3] A. Liénard, Etude des oscillations entrenues, *Revue Génerale de l'Ělectricité* 23 (1928) 946–954.
[4] S. Lynch, Liénard systems and the second part of Hilbert's sixteenth problem, *Nonlinear Analysis, Theory, Methods and Applications* 30 (1997) 1395–1403.
[5] S.H. Chen, Y.K. Cheung, An elliptic perturbation method for certain strongly non-linear oscillators, *Journal of Sound and Vibration* 192 (1996) 453–464.
[6] Y.K. Cheung, S.H. Chen, S.L. Lau, A modified Lindstedt–Poincaré method for certain strongly non-linear oscillators, *International Journal of Non-Linear Mechanics* 26 (1991) 367–378.
[7] J. Garcia-Margallo, J.D. Bejarano, The limit cycles of the generalized Rayleigh–Liénard oscillator, *Journal of Sound and Vibration* 156 (1992) 283–301.
[8] J. Garcia-Margallo, J.D. Bejarano, The greatest number of limit cycles of the generalized Rayleigh–Liénard oscillator, *Journal of Sound and Vibration* 221 (1) (1999) 133–142.
[9] W. Zhang, P. Yu, A study of the limit cycles associated with a generalized codimension-3 Liénard oscillator, *Journal of Sound and Vibration* 231 (1) (2000) 145–173.
[10] S. Lynch, C.J. Christopher, Limit cycles in highly non-linear differential equations, *Journal of Sound and Vibration* 224 (3) (1999) 505–517.
[11] N. Ananthkrishnan, K. Sudhakar, S. Sudershan, A. Agarwal, Application of secondary bifurcations to large amplitude limit cycles in mechanical systems, *Journal of Sound and Vibration* 215 (1) (1998) 183–188.
[12] M. Golubitsky, D.G. Schaeffer, *Singularities and Groups in Bifurcation Theory*, Vol. 1, Springer, New York, 1985.
[13] C. Yushu, A.Y.T. Leung, *Bifurcation and Chaos in Engineering*, Springer, London, 1998.
[14] A.H. Neyfeh, D.T. Mook, *Nonlinear Oscillations*, Wiley, New York, 1979.